Novel mathematical and statistical approaches to uncertainty evaluation:

Conformity assessment for computationally expensive systems : application to fire safety engineering

Deliverable 3.2.6
of Work Package
WP3 (Decision-making and conformity assessment)

Authors:

Séverine Demeyer, Damien Marquis
Laboratoire National de Métrologie et d'Essais, F

A report of the EMRP joint research project
NEW04 "Novel mathematical and statistical approaches to uncertainty evaluation"

1. Work package	2. Deliverable number	3. Reporting date
WP 3	D3.2.6	May 2015

4. Title
Conformity assessment for computationally expensive systems : application to fire safety engineering

5. Author(s)
Séverine Demeyer (F), Damien Marquis (F)

6. Lead author (e-mail)
severine.demeyer@lne.fr

7. Contributing researchers (institutes)
LNE (F)

8. Other contributing work packages
D3.1.3, D3.1.4, D3.2.5

9. Researchers in other WPs

10. Supplementary notes
None

11. Abstract
This document reports a guide for conformity assessment of computationally expensive systems using cheaper approximations. Modelling the relationship between the two codes and the behaviour of the codes viewed as black boxes evaluated at input points using co-kriging, provides a probabilistic framework to assess the probability of conformity of the expensive system with an associated uncertainty. In order to increase the accuracy of the probability of non conformity with a limited number of new runs, a procedure is derived to sequentially sample smart new points targeting the non conformity domain. The approach is illustrated on a fire engineering case study, in which the probability of conformity of a smoke control device is assessed by combining expensive CFD simulations (code FDS) with cheap code approximations (code CFAST).

12. Key words
Monte Carlo Method, co-kriging, sequential sampling, probability of exceeding threshold, fire engineering

Contents

1 Introduction **1**

2 Assessing conformity in fire safety engineering **1**
2.1 Fire engineering case study : context and tenability criteria . . . 1
2.2 Fire model . . . 2
2.2.1 Zone model - CFAST . . . 2
2.2.2 Computational fluid dynamics model - FDS . . . 2
2.3 Input data . . . 3
2.4 Output data . . . 5

3 Methodology to assess the probability of non conformity of computationally expensive systems using fast approximations **7**
3.1 Conformity of a computationally expensive system . . . 7
3.2 Initial design of experiments . . . 7
3.3 Co-kriging metamodel . . . 8
3.4 Estimation of a co-kriging metamodel . . . 8
3.5 Prediction from a co-kriging model . . . 9
3.6 Computation of the probability of non conformity of an expensive system . . . 9
3.6.1 Probability of excursion . . . 9
3.6.2 Probability of exceeding a threshold . . . 9
3.7 Sequential co-kriging . . . 10

4 Application to the fire engineering case study **11**
4.1 Sensitivity analysis . . . 11
4.2 Monte Carlo baseline results . . . 12
4.3 Kriging and co-kriging models . . . 12
4.4 Numerical interpretation of the results . . . 13
4.5 Graphical interpretation of the sequential co-kriging results . . . 14

5 Conclusion **16**

Acknowledgements **16**

List of Figures

1 Simulation of fire plume in a building. Numerical room with the CFD code Fire Dynamics Simulator. Smoke plume obtained from a fire area of $13.75m^2$ and a heat release rate of $487kW.m^{-2}$. Dummy regions and layer height are represented. 3
2 Sample design fire curve. 4
3 Iso-temperature located at the term source ($y = 0$) at $t = 200s$ Results obtained from a fire area of $13.75m^2$ and a heat release rate of $487kW.m^{-2}$. 6
4 Flowchart of the sequential co-kriging procedure. 12
5 Initial database and initial level plot of the probability of excursion function. In green, the points that are only evaluated by CFAST; in red, the points that are evaluated by CFAST and FDS. 13
6 Contour plot of the initial probability of excursion (a) and the updated probability of excursion after 2 points have been added at the first iteration of the sequential co-kriging procedure (b). . 15
7 Contour plot of the updated probability of excursion at the second iteration of the sequential co-kriging procedure (a) and at the third iteration (b). 16

List of Tables

1 Description of the input variables of the fire code (N: normal, U: uniform). 5
2 Summary results of the probability of non conformity $\hat{p}_f$, its associated uncertainty $u(\hat{p}_f)$ and its coefficient of variation (relative uncertainty) $cv(\hat{p}_f)$ obtained with various kriging based methods. 14
3 Summary results of the probability of non conformity $\hat{p}_f$, its associated uncertainty $u(\hat{p})$ and its coefficient of variation (relative uncertainty) $cv(\hat{p}_f)$ obtained at each iteration of the sequential procedure. Iteration 0 gives the baseline results obtained with the initial database (9 points). . 15

1 Introduction

When dealing with a computational code, one may be interested in propagating the uncertainties related to the input variables to estimate the uncertainty associated with the output variable.

In the decision theoretical framework pertaining to conformity assessment, one is interested also in the position of the output variable with respect to a given threshold (regulatory threshold,...). The problem of knowing whether a computationally expensive model exceeds a given threshold is very common for reliability analysis and safety-critical applications such as aerospace, nuclear power stations and civil engineering (models of bridges and buildings etc). The threshold can be interpreted as a lower specification limit defining a one-sided tolerance interval.

In this guide, the decision is based on the probability that the output exceeds the threshold. Accordingly, the decision of conformity is based on the probability of conformity.

An alternative approach could be to estimate the 5% quantile of the output distribution and compare it to the lower specification limit as proposed in [1].

The statistical methods that are usually used to deal with the propagation of uncertainties may need to be adapted to compute the probability of exceeding a threshold. This is particularly the case when the probability is small or when the code is computationally expensive.

This document reports a guide for conformity assessment of computationally expensive systems using cheaper approximations based on odelling the relationship between the two codes and the behaviour of the codes viewed as black boxes evaluated at input points using co-kriging.

Section 2 reports conformity assessment in fire safety engineering and describes the fire engineering case study. Section 3 describes the statistical methodology to take advantage of cheaper approximations when assessing the conformity of an expensive system. Section 4 applies the methodology to the fire engineering case study and compares results obtained with various kriging methods.

2 Assessing conformity in fire safety engineering

2.1 Fire engineering case study : context and tenability criteria

For fire safety engineer, one of the major problem consists to limit the fire risk in a large spaces such as buildings, shopping malls, car park, theaters, etc. The strategy adopted consists to reduce its occurrence and the design fire load or to limit its extent through the use of fire suppression systems such as sprinklers [2]. This approach is currently achieved by a second line of defense which consist to ensure that the thermal stratification is high enough so that occupant are not trapped in the smoke and may escape easily to a place of refuge. In other words, the objective is therefore to guarantee that the environment at heights useful for evacuation is clear enough to allow occupant to evacuate before reaching compromised tenability conditions in term of heat and toxicity of smoke. In order to achieve this objective, adapted smoke removal systems are used in order to keep the thermal stratification at a sufficient height for a time long enough.

The prediction of the evolution of tenability condition in an environment in fire can be estimated using complex fire model like zone model or computational fluid dynamics tool. It require also to set appropriate tenability criteria which ensure that the occupants will not be exposed to untenable conditions. Nowadays, there is no single set that is universally accepted and various tenability criteria are proposed [3]. The tenability criteria used in the present study come from the international standard ISO 13571 [4]. They are based on the best available scientific judgement of the consequences of human exposure to fire effluents. According to this standard, during the people evacuation, the risks related to fire mainly of three types:

- The loss of visibility can cause delay in escape, disorientate the crowds and can expose them for longer

periods of time or induce significant exposure to the other effects of fire;

- The thermal risks generated by fire and smoke can lead to incapacitation or lethality among populations. They are linked to the heat flux associated to the radiation of the smoke and the temperature of the atmosphere;
- The toxic risks related to the chemical species present in smoke. These are incapacitating or can be lethal, sometimes at considerable distances from the fire.

Given the numerical tool used, and in order to simplify the problem, one decided that the modelling focuses only on the life threat due to heat exposure. In this case, only two criteria are considered :

- the threshold of second degree burning of the skin. The tenability limit for exposure of skin to radiant heat is approximately $2.5\ kWm^{-2}$. Below this incident heat flux level, exposure can be tolerated for $30\ min$ or longer without significantly affecting tenability. It can be noted that the radiant heat limit of $2.5\ kWm^{-2}$ may be reached when the hot layer temperature rises above $200°C$. Furthermore, thermal burns to the respiratory tract can occur upon inhalation of air above $60\ °C$ when saturated with water vapour.
- the exposure where hyperthermia is sufficient to cause mental deterioration and, therefore, threaten survival. Thermal tolerance data for unprotected skin of humans suggest a limit of about $120\ °C$ for convected heat, above which there is, within minutes, the onset of considerable pain along with the production of burns [[4]].

From the above description, in fire safety studies, the typical methods for ensuring whether the environment on the evacuation path is practicable enough to allow occupant to locate emergency exit, consist to check that the fields are roughly uniform at height 2m (except obviously in the fire plume) [2]. Then it must be ensured that the radiant heat from the fire and the hot smoke layer does not exceed the skin pain threshold of $2.5\ kWm^{-2}$ (and therefore $T < 200\,°C$). Finally the last criterion lead to ensure that the temperature at nose height ($1.5\,m$) do not exceed $60\ °C$.

2.2 Fire model

2.2.1 Zone model - CFAST

The Consolidated Model of Fire and Smoke Transport, CFAST, is a numerical tool use to simulate the impact of past or potential fires and smoke in a specific building environment. CFAST is a fire model which relies on the assumption that a volume is subdivided in a two-zone zones, perfectly mixed and with homogeneous properties in terms of temperature and composition: a hot layer with combustion products, located near the ceiling, and a cold layer with fresh clean air at the bottom, separated by a moving interface. The fundamental equations (conservation of mass and energy, ideal gas law and internal energy) are implemented as a system of ordinary differential equations (ODE). These ODE are solved to give the evolving distribution of pressure, layer heights and temperatures. Zone models rely on very strong simplifications and their application is limited to the geometry characteristics over which the model was tested and validated. For further details on CFAST, the reader is referred to the ref. [5] .

2.2.2 Computational fluid dynamics model - FDS

CFD simulations were performed with the version 6.1.2 of the Fire Dynamics Simulator (FDS) code developed by the NIST Building and Fire Research Laboratory (USA) and the VTT technical research centre of Finland.

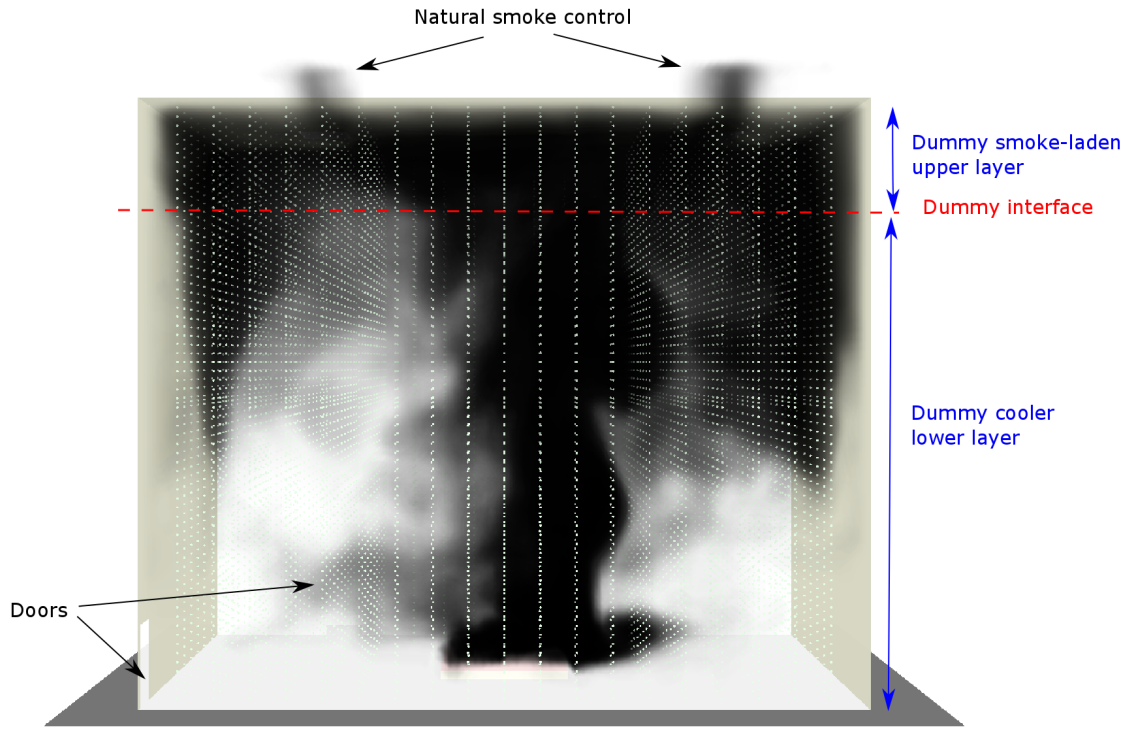

Figure 1: Simulation of fire plume in a building. Numerical room with the CFD code Fire Dynamics Simulator. Smoke plume obtained from a fire area of $13.75m^2$ and a heat release rate of $487kW.m^{-2}$. Dummy regions and layer height are represented.

FDS solves an approximation of the Navier-Stokes equations appropriate for low-mach number, thermally-driven flows. The numerical algorithm employed is an explicit predictor/corrector scheme, second order accurate both in space and time, using a direct Poisson solver. Turbulence is treated using Large Eddy Simulation (LES), via the classical Smagorinsky subgrid scale model. A mixture fraction combustion model assuming an infinitely fast global chemical reaction is used to estimate the heat release and smoke distributions in the computational domain. The radiation transport is treated using a finite volume solver in which grey gas absorption coefficient for soot and gas species is linked to the mixture fraction. FDS relies on strong assumptions which limit the application to well-ventilated fire. For further details on FDS, the reader is referred to the ref. [6].

2.3 Input data

For the purpose of the study, a known building is considered. As a consequence, its dimensions are known (dimensions: $19.75m$(length)$\times$ $12m$ (width)$\times$ $16.50m$(height)) along with those of the openings with negligible uncertainty. These quantities are then assigned a fixed value. The thickness and the thermal properties of the walls are defined in accordance with the present structures. The test hall is equipped with two doors assumed as open (dimensions: m (length) $\times$ m(width)) and two natural smoke removal system (dimensions : m (length) $\times$ m(width)). The room mesh is defined from the actual dimensions of the test hall, as shown in Fig. 1. In the case of FDS, the grid is uniform, and the cell dimensions are 25 cm on each side. This cell size is a compromise between flow resolution and computational time.

As the boundary condition, the gas in the computation domain was set still with ambient temperature. At the free side, static pressure boundary condition was employed. The fire source is placed in the centre of the

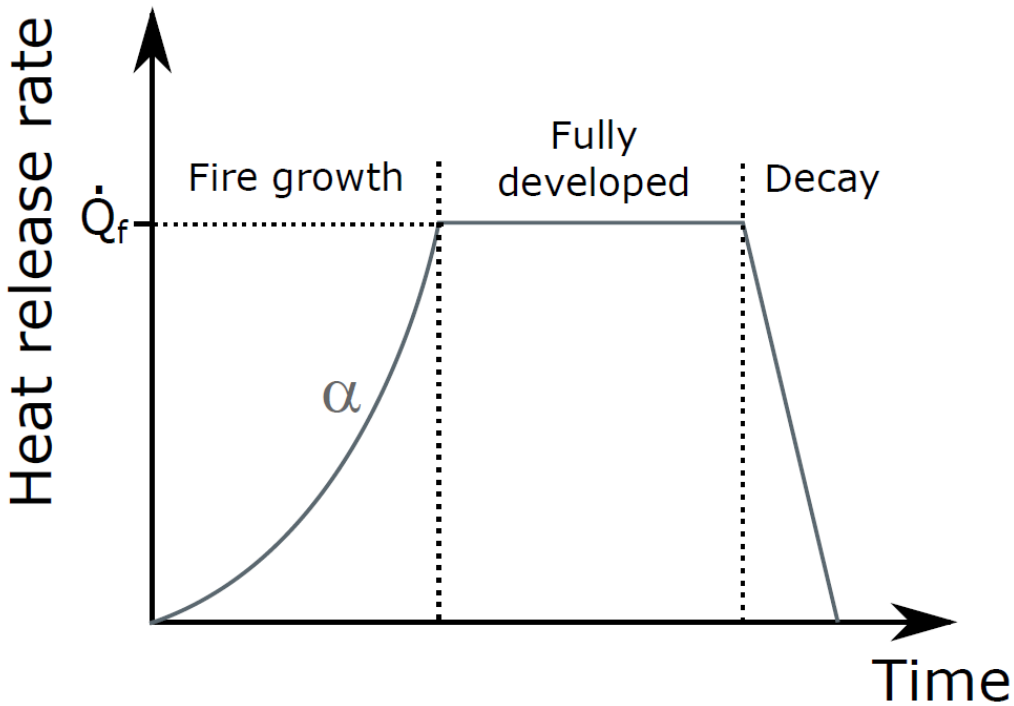

Figure 2: Sample design fire curve.

test hall.

Apart from changes in environmental conditions (such as outside and inside temperatures, ambient pressure and relative humidity, wind velocity and direction), the properties of the fire (fire source area, fire growth rate and heat release rate per unit area) in the hall test is governed by the physical and chemical process evolved. Multiple interactions between these input variables at different time during the fire may affect the pattern of the fire growth and lead to uncertainties. For this reason, there is a need to determine the uncertainty (probability) with which input variables may affect a real fire in a known building. In the present framework, the environmental conditions and the properties of the fire are therefore randomly determined. The chosen probability distributions for these input variables are detailed in Table 2.

The fire scenarios (fire area, heat release rate per unit area and fire growth rate) are not deduced from a specific analysis of the considered test hall. They are representative of the scenarios commonly validated in the context of the studies in fire safety engineering, according to the French regulation. In the smoke control chapter of this regulation, the fire to be taken into account to assess smoke removal systems is conventionally defined as a fire area called A_f [7] whose surface may be $9\,m^2$, $18\,m^2$, $36\,m^2$ depending on the main purpose of the building. In the present study, a fire area from $9\,m^2$ to $36\,m^2$ have been considered using an uniform law.

The fire power is classically associated with the heat release rate per unit area $\dot{Q}''_f$ and its evolution is usually described by empirical design fire curves (Fig. 2) describing a growth step, a steady state and a decay period. For smoke control engineering studies, usage is to consider $\dot{Q}''_f$ that lies between $300\,kW.m^{-2}$ and $500\,kW.m^{-2}$, which correspond to a fire of $300\,kW$ to $18\,MW$. The bounds have been kept for this study. The chosen associated law is an uniform one. According to Alpert [8], the rate of fire development, shown on Fig. 2, can be approximated by a parabolic growth ('t^2' time) after the ignition reference time t_i as follow:

$$\dot{Q}_f = \alpha(t - t_i)^2 \tag{1}$$

where α is a fire growth coefficient ($kW.s^{-2}$), and t the time (s). The coefficient α varies between $0.011338 kW.s^{-2}$ for a very slowly developing fire and $0.2\ kW.s^{-2}$ for very fast fire growth [9]. The chosen associated law is an uniform one.

The fire load densities were typically presented in MJ per unit area of the surfaces bounding the fire building, as follow:

$$q''_f = \int_{t_i}^{t_e} \dot{Q}''_f dt \tag{2}$$

In the present case, the value of q''_f have an impact of the combustion duration. Usage is to consider q''_f that lies between $300\ MJ.m^{-2}$ and $500\ MJ.m^{-2}$. The chosen associated law is an uniform one.

The probability distributions for the environmental conditions are also representative of the climatic conditions encountered in France all over the year. Outside mean temperature (denoted as T_{ext}) could vary between $-20\,°C$ and $+40\,°C$, which are mean extreme values found in France according to meteorological survey. The chosen distribution law is normal with a standard deviation equal to the third of the semi length of the interval of variation. Inside temperature (denoted as T_{int}) could vary between $+15°C$ and $+27°C$ according to extrema found in ISO 7730 standard [10]. The chosen distribution law is normal with a standard deviation equal to the third of the semi length of the interval of variation. For simplicity purposes, the effects on the wind are not considered in this study. Finally, each input quantity is supposed to be independent.

Table 1: Description of the input variables of the fire code (N: normal, U: uniform).

Variable	Name	Unit	Range	Distribution
P_{atm}	Atmospheric pressure	Pa	$[98000, 102000]$	N
T_{ext}	External temperature	K	$[263.15, 303.15]$	N
T_{int}	Inside temperature	K	$[290, 303.15]$	N
α	Fire growth rate	kW.s^{-2}	$[0.011338, 0.20]$	U
A_f	Fire area	m^2	$[1, 20]$	U
$\dot{Q}''_f$	Characteristic HRR per unit area	kW.m^{-2}	$[300, 500]$	U
q''_f	Design fire load density per unit area	MJ.m^{-2}	$[300, 600]$	U

2.4 Output data

In the present study, the variables of interest are three parameters (see Fig. 1) which allow to evaluate when the building environment reaches compromised tenability conditions: the smoke-laden upper layer temperature T_U; the lower layer temperature T_L; and the position of this interface, also called layer height Z_{int}. These parameter can be easily estimated from two-zone models like CFAST, as it computes this quantity directly, along with the average temperature of the upper and lower layers. In a CFD model like FDS, it is far more complex because there are not two distinct zones, but rather a continuous profile of temperature [6], as illustrated on Fig. 3.

Janssens [11] proposes a method to estimate the layer height and the average temperatures from a continuous vertical profile of temperature. From this approach, FDS considers a continuous function T(z) defining

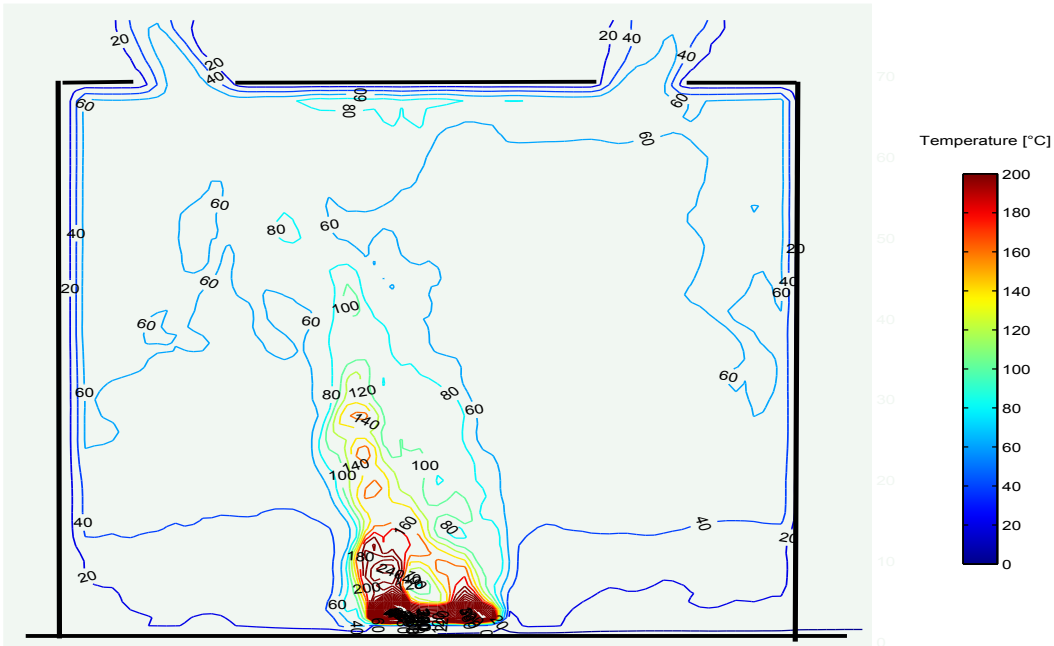

Figure 3: Iso-temperature located at the term source ($y = 0$) at $t = 200s$ Results obtained from a fire area of $13.75m^2$ and a heat release rate of $487kW.m^{-2}$.

temperature T as a function of height above the floor z, where $z = O$ is the floor and $z = H$ is the ceiling. FDS estimates these quantities:

$$(H - z_{int})\, T_U + z_{int}\, T_L = \int_0^H T(z)\, dz = C_1 \tag{3}$$

$$(H - z_{int})\, \frac{1}{T_U} + z_{int}\, \frac{1}{T_L} = \int_0^H \frac{1}{T(z)}\, dz = C_2 \tag{4}$$

and resolves this equation in order to estimate the position of the interface

$$z_{int} = \frac{T_L(C_1\, C_2 - H^2)}{C_1 + C_2\, T_L^2 - 2\, T_L\, H} \tag{5}$$

Finally T_U is defined as the average upper layer temperature from:

$$(H - z_{int})\, T_u = \int_{z_{int}}^H T(z)\, dz. \tag{6}$$

Further discussion of similar procedures can be found in Ref. [12].

In order do not affect the results, these sensors used to measure T_U, T_L and z_{int}, are not directly positioned in the fire plume.

As these quantities evolve during the fire, one consider here as measurand the maximal value obtained throughout the simulation for the upper and lower layer temperature and the minimal value of the layer height z_{int}.

3 Methodology to assess the probability of non conformity of computationally expensive systems using fast approximations

3.1 Conformity of a computationally expensive system

The probabilistic model associated to numerical experiments is defined as $Y_i = F(\boldsymbol{X_i})$, $i = 1, ..., L$ where F denotes the computational code (black box) and $\boldsymbol{X_i} = (X_{i1}, ..., X_{iK})^T$ denotes the column vector of K input variables, Y_i is the model output and L is the number of runs of the code.

Let us denote $\mathcal{D}$ the domain of variation of the K input variables.

When dealing with a computationally expensive code with only a small number of simulations possible in the time of a study, it may be useful to use a faster code and to find the relation (if any) between these cheap approximations and the expensive more accurate ones through a statistical model.

By increasing the size of the data and using Monte Carlo simulations from the statistical model, this approach allows to compute indicators and their associated uncertainties that would be intractable otherwise. As such, the conformity of an expensive system can now be evaluated as a probability of conformity with an associated uncertainty, which will lead to a more reliable decision indicator.

Given a critical output quantity and a regulatory threshold, the probability of non conformity is the probability that the expensive (and assumed more reliable) code output exceeds the threshold, and reads

$$p_f = P\left(\{\boldsymbol{x} \in \mathcal{D} : F(\boldsymbol{x}) > s\}\right) = \int 1_{F(\boldsymbol{x})>s} f(\boldsymbol{x}) d\boldsymbol{x} \tag{7}$$

where f is the joint density of the input variables defined on the domain $\mathcal{D}$, $1_{F(\boldsymbol{x})>s} = 1$ if $F(\boldsymbol{x}) > s$ and $1_{F(\boldsymbol{x})>s} = 0$ otherwise.

3.2 Initial design of experiments

Denote $\mathcal{D}_1 = (\boldsymbol{x}_{11}, ..., \boldsymbol{x}_{1n_1})$ and $\mathcal{D}_2 = (\boldsymbol{x}_{21}, ..., \boldsymbol{x}_{2n_2})$ the designs of experiments at the lower level (fast computations) and at the higher level (expensive computations) respectively, with $\mathcal{D}_2 \subset \mathcal{D}_1 \subset \mathcal{D}$ where $\mathcal{D}$ is the domain of variation of the input variables.

Let $\boldsymbol{y}^{\mathrm{T}} = (\boldsymbol{y}_1^{\mathrm{T}}, \boldsymbol{y}_2^{\mathrm{T}})$ be the output data, where $\boldsymbol{y}_1^{\mathrm{T}} = F_1(\mathcal{D}_1) = (F_1(\boldsymbol{x}_{11}), ..., F_1(\boldsymbol{x}_{1n_1}))$ and $\boldsymbol{y}_2^{\mathrm{T}} = F_2(\mathcal{D}_2) = (F_2(\boldsymbol{x}_{21}), ..., F_2(\boldsymbol{x}_{2n_2}))$ denote the outputs of the codes F_1 (fast approximations) and F_2 (expensive runs) respectively.

If information or an educated guess are available about the failure domain, some of the points or some of the coordinates of the points should be fixed accordingly. The remaining points or the initial designs of experiments should explore the input space and can be obtained with nested latin hypercube designs.

The number of initial points and their distribution on either the higher level or the lower level code depends on a compromise between the time of a run at each level and its relevance to evaluate the failure probability (which depends on the number of input variables and the sought probability). If higher level experiments are too expensive, lower level experiments can be used to predict initial failure points to be evaluated at the higher level.

3.3 Co-kriging metamodel

For $\boldsymbol{x} \in \mathcal{D}$, the co-kriging metamodel is defined as

$$\tilde{y}_2(\boldsymbol{x}) = \rho \tilde{y}_1(\boldsymbol{x}) + \delta(\boldsymbol{x}) \tag{8}$$

The parameter ρ can be interpreted as a regression parameter between the surrogate outputs $\tilde{y}_1(.)$ and $\tilde{y}_2(.)$ of the codes F_1 and F_2 respectively. The term $\delta(.)$ controls the variability of $\tilde{y}_2(.)$ that is not explained by $\tilde{y}_1(.)$ and is independent from $\tilde{y}_1(.)$.

Conditional on hyperparameters β_2, σ_δ^2 and ψ_2, $\delta(.)$ is modelled as a Gaussian process with mean $m_\delta(.) = h(.)^T\beta_2$ and covariance function $k_\delta(\boldsymbol{x}, \boldsymbol{x}') = \sigma_\delta^2 r_\delta(\boldsymbol{x}, \boldsymbol{x}'; \psi_2)$. For $\boldsymbol{x} = \boldsymbol{x}'$, $k_\delta(\boldsymbol{x}, \boldsymbol{x}') = \sigma_\delta^2$ the variance of the process $\delta(.)$.

Conditional on hyperparameters β_1, σ_1^2 and ψ_1, $\tilde{y}_1(.)$ is modelled as a Gaussian process with mean $m_1(.) = h(.)^T\beta_1$ and covariance function $k_1(\boldsymbol{x}, \boldsymbol{x}') = \sigma_1^2 r(\boldsymbol{x}, \boldsymbol{x}'; \psi_1)$. For $\boldsymbol{x} = \boldsymbol{x}'$, $k_1(\boldsymbol{x}, \boldsymbol{x}') = \sigma_1^2$ the variance of the process $\tilde{y}_1(.)$.

As a consequence of model (8), $\tilde{y}_2(.)$ is a Gaussian process with mean $m_2(\boldsymbol{x}) = h'(\boldsymbol{x})^T\beta$ with $h'(\boldsymbol{x})^T = \left(\rho h(\boldsymbol{x})^T, h(\boldsymbol{x})^T\right)$ and $\beta^T = (\beta_1^T, \beta_2^T)^T$, and covariance function $k_2(\boldsymbol{x}, \boldsymbol{x'}) = \rho^2 k_1(\boldsymbol{x}, \boldsymbol{x'}) + k_\delta(\boldsymbol{x}, \boldsymbol{x'})$. It follows that the prior variance of the process $\tilde{y}_2$ is obtained as $k_2(\boldsymbol{x}, \boldsymbol{x}) = \rho^2\sigma_1^2 + \sigma_\delta^2$.

3.4 Estimation of a co-kriging metamodel

For $t = \{1, 2\}$ let us denote $h(\mathcal{D}_t) = \left(h(\boldsymbol{x}_{t1})^T, ..., h(\boldsymbol{x}_{tn_t})^T\right)^T$ the column vector of the regression functions of the code level t evaluated at points in $\mathcal{D}_t$. The regression functions h_1 and h_2 evaluated at data points $\boldsymbol{y}$ form the block matrix H as follows

$$H = \begin{pmatrix} h(\mathcal{D}_1) & 0 \\ \rho h(\mathcal{D}_2) & h(\mathcal{D}_2) \end{pmatrix} \tag{9}$$

For $t = \{1, 2\}$ let us denote $k_t(\mathcal{D}_1, \mathcal{D}_2) = \{k_t(\boldsymbol{x}, \boldsymbol{x'}), \boldsymbol{x} \in \mathcal{D}_1, \boldsymbol{x}' \in \mathcal{D}_2\}$ the correlation matrix between points in $\mathcal{D}_1$ and $\mathcal{D}_2$ and let us use the shorthand $k_t(\mathcal{D}_t) = k_t(\mathcal{D}_t, \mathcal{D}_t)$ to denote the correlation matrix between points in $\mathcal{D}_t$. Note that $k_t(\mathcal{D}_1, \mathcal{D}_2) = k_t(\mathcal{D}_2, \mathcal{D}_1)$.

The covariance matrix V of the data points $\boldsymbol{y}$ can be expressed as the following block matrix

$$V = \begin{pmatrix} \sigma_1^2 k_1(\mathcal{D}_1) & \rho\sigma_1^2 k_1(\mathcal{D}_1, \mathcal{D}_2) \\ \rho\sigma_1^2 k_1(\mathcal{D}_1, \mathcal{D}_2) & \rho^2\sigma_1^2 k_1(\mathcal{D}_2) + \sigma_2^2 k_2(\mathcal{D}_2) \end{pmatrix} \tag{10}$$

It ensues that the likelihood of data points $\boldsymbol{y}$ is given by

$$\boldsymbol{y} \sim N(H\boldsymbol{\beta}, V) \tag{11}$$

Denoting $\Theta = \left\{\rho, \boldsymbol{\beta}, \psi_1, \psi_2, \sigma_1^2, \sigma_\delta^2\right\}$ the collection of co-kriging parameters, yields the following analytical expression of the likelihood

$$l(\boldsymbol{y}|\Theta) \propto \exp\left\{-\frac{1}{2}(\boldsymbol{y} - H\boldsymbol{\beta})^T V^{-1}(\boldsymbol{y} - H\boldsymbol{\beta})\right\} \tag{12}$$

Following the approach presented in [13], the parameters of the covariance functions $\psi_1, \psi_2, \sigma_1^2, \sigma_\delta^2$ and the coefficient ρ are estimated by maximum likelihood. Denote $\hat{\phi} = \left(\hat{\rho}, \hat{\psi}_1, \hat{\psi}_2, \hat{\sigma}_1^2, \hat{\sigma}_2^2\right)$ the vector of maximum likelihood estimates of the vector of parameters $\left(\rho, \psi_1, \psi_2, \sigma_1^2, \sigma_2^2\right)$ given the observations $\boldsymbol{y}$.

The parameters $\boldsymbol{\beta}$ are estimated with a Bayesian approach under the non informative prior distribution $p(\boldsymbol{\beta}) \propto 1$ conditionnally on the observed data $\boldsymbol{y}$ and the estimated vector $\hat{\phi}$.

The posterior mean $\hat{\boldsymbol{\beta}}$ of $\boldsymbol{\beta}$ is obtained as $\hat{\boldsymbol{\beta}} = \left(H^T V^{-1} H\right)^{-1} H^T V^{-1} \boldsymbol{y}$.

3.5 Prediction from a co-kriging model

The aim is to predict values of the higher level code F_2 at untried input values $\boldsymbol{x}$. Credible values for $F_2(\boldsymbol{x})$ given the observed data $\boldsymbol{y}$ and the estimated parameters and their uncertainties are embedded in the posterior predictive distribution $[\tilde{y}_2(\boldsymbol{x})|\boldsymbol{y}]$.

Following [13], $[\tilde{y}_2(\boldsymbol{x})|\boldsymbol{y}]$ is a Gaussian Process with mean function $m_{2,co}(.)$ and covariance function $k_{2,co}$ with

$$m_{2,co}(\boldsymbol{x}) = h'(\boldsymbol{x})\hat{\beta} + r(\boldsymbol{x})^T V^{-1}\left(\boldsymbol{y} - H\hat{\beta}\right) \tag{13}$$

$$\begin{aligned} k_{2,co}(\boldsymbol{x}, \boldsymbol{x'}) = k_2(\boldsymbol{x}, \boldsymbol{x'}) - r(\boldsymbol{x})^T V^{-1} r(\boldsymbol{x}) \\ + (h'(\boldsymbol{x}) - r(\boldsymbol{x})V^{-1}H)^T (H^T V^{-1} H)^{-1} (h'(\boldsymbol{x}) - r(\boldsymbol{x})^T V^{-1} H) \end{aligned} \tag{14}$$

where $r(\boldsymbol{x})^T = \mathrm{cov}\{\tilde{y}_2(\boldsymbol{x}), \boldsymbol{y}^T\} = \left(\rho\sigma_1^2 k_1(\boldsymbol{x}, \mathcal{D}_1), \rho^2\sigma_1^2 k_1(\boldsymbol{x}, \mathcal{D}_2) + \sigma_2^2\right) k_2(\boldsymbol{x}, \mathcal{D}_2)$ is the row vector of covariance between $\tilde{y}_2(\boldsymbol{x})$ and the observed data $\boldsymbol{y}^T$ and $h'(\boldsymbol{x})^T = \left(\rho h(\boldsymbol{x})^T, h(\boldsymbol{x})^T\right)$ is the row vector of regression functions evaluated at $\boldsymbol{x}$.

3.6 Computation of the probability of non conformity of an expensive system

In this section, we denote $\tilde{y}(.)$ the estimated kriging metamodel of an expensive system F obtained either by direct kriging of the code, or by co-kriging of two codes. In this latter case, we set $\tilde{y}(.) = [\tilde{y}_2(.)|\boldsymbol{y}]$ the kriging model used to predict the outputs at the higher level F_2 derived at section 3.5. We also denote $\hat{m}(\boldsymbol{x}) = E(\tilde{y}(\boldsymbol{x}))$ and $\hat{\sigma}^2(\boldsymbol{x}) = E\left((\tilde{y}(\boldsymbol{x}) - \hat{m}(\boldsymbol{x}))^2\right)$ the predicted mean and variance at point $\boldsymbol{x}$ respectively.

3.6.1 Probability of excursion

The probability of excursion $\pi(\boldsymbol{x})$ is defined for location $\boldsymbol{x} \in \mathcal{D} \setminus \mathcal{D}_n$ as

$$\pi(\boldsymbol{x}) = P\left(\tilde{y}(\boldsymbol{x}) > s\right) = P\left(\frac{\tilde{y}(\boldsymbol{x}) - \hat{m}(\boldsymbol{x})}{\hat{\sigma}(\boldsymbol{x})} > \frac{s - \hat{m}(\boldsymbol{x})}{\hat{\sigma}(\boldsymbol{x})}\right) = \Phi\left(\frac{\hat{m}(\boldsymbol{x}) - s}{\hat{\sigma}(\boldsymbol{x})}\right) \tag{15}$$

where Φ is the cumulative distribution function of the standard Gaussian distribution.

Note that the probability of excursion is not the sought probability of conformity.

3.6.2 Probability of exceeding a threshold

The probability of non conformity p_f of a computationally expensive system approximated by a metamodel $\tilde{y}(.)$ is given by

$$p_f = \int 1_{\tilde{y}(\boldsymbol{x}) > s} f(\boldsymbol{x}) d\boldsymbol{x} \tag{16}$$

The best estimator $\hat{p}_f$ of p_f that minimizes the mean squared error $MSE := E_{\tilde{y}}\left((p_f - \hat{p}_f)^2\right)$ is (see [14])

$$\hat{p}_f = E_{\tilde{y}}\left(p_f\right) = \int P\left(\tilde{y}(\boldsymbol{x}) > s\right) f(\boldsymbol{x}) d\boldsymbol{x} = \int \pi(\boldsymbol{x}) f(\boldsymbol{x}) d\boldsymbol{x} \tag{17}$$

where $\pi(.)$ is the probability of excursion defined in (15).

A measure of uncertainty associated to this estimator is

$$u^2\left(\hat{p}_f\right) = E_{\tilde{y}}\left(\left(p_f - \hat{p}_f\right)^2\right) = MSE \tag{18}$$

For computational reasons the estimators (17) and (18) are computed with Monte Carlo simulations.

Computation of $\hat{p}_f$ A Monte Carlo method has been proposed in [15] that relies on sampling realizations (trajectories) $\tilde{y}_{(k)}(.)$ of the Gaussian Process $\tilde{y}(.)$.

$$\hat{p}_f \approx \frac{1}{K} \sum_{k=1}^{K} p_{f,(k)} \tag{19}$$

where $p_{f,(k)} = P\left(\tilde{y}_k > T\right) = \int_{\mathcal{D}} 1_{\tilde{y}_k(\boldsymbol{x}) > T} f\left(\boldsymbol{x}\right) \mathrm{d}\boldsymbol{x}$.

For a given trajectory k, a Monte Carlo estimation $\hat{p}_{f,(k)}$ of $p_{f,(k)}$ reads

$$\hat{p}_{f,(k)} = \frac{1}{L} \sum_{l=1}^{L} 1_{\hat{m}_{(k)}(\boldsymbol{x}_l) > T} \tag{20}$$

for $\boldsymbol{x_1}, ..., \boldsymbol{x_L}$ having density f.

Combining (19) and (20) gives the Monte Carlo estimate of the probability of non conformity

$$\hat{p_f} \approx \frac{1}{KL} \sum_{k=1}^{K} \sum_{l=1}^{L} 1_{\hat{m}_{(k)}(\boldsymbol{x}_l) > T} \tag{21}$$

Computation of $u\left(\hat{p}_f\right)$

$$u^2\left(\hat{p}_f\right) \approx \frac{1}{K} \sum_{k=1}^{K} \left(\hat{p}_{f,(k)} - \hat{p}_f\right)^2 \tag{22}$$

where $\hat{p}_{f,(k)}$ is defined in (20) and $\hat{p_f}$ is defined in (21).

The Monte Carlo estimate of the measure of uncertainty associated with the probability of conformity (18) finally reads

$$u^2\left(\hat{p}_f\right) = \frac{1}{K} \sum_{k=1}^{K} \left(\frac{1}{L} \sum_{l=1}^{L} 1_{\hat{m}_{(k)}(\boldsymbol{x_l}) > s} - \hat{p}_c\right)^2 \tag{23}$$

3.7 Sequential co-kriging

Sequential co-kriging consists in sequentially adding points to the database that will be evaluated by the two code levels to decrease the relative uncertainty (coefficient of variation) of the estimated probability of non conformity.

Sequentially adding points to a learning database (also called sequential planning) according to a space filling design brings a global reduction of uncertainty (see [16]). However this approach is not necessarily pertaining to the problem of determining the failure area and its probability accurately. Indeed when the target

area has a low probability, points have a very low probability to fall in. This is particularly critical in high dimensional problems.

Specific sequential methods targeting the failure area are required. Such methods have already been developed to estimate a probability of failure based on a kriging model of a computer code (see [14] and [17]). Since the posterior predictive distribution of $\tilde{y}_2(.)|\boldsymbol{y}$ is a Gaussian process such methods can be applied to $\tilde{y}_2(.)|\boldsymbol{y}$.

Among others, we present and use in the application the targeted Mean Square Error (tMSE) criterion. Given a current Gaussian process and a current database of n points, the one-at-a-time version of the criterion allows to select the $n+1$th point as the point satisfying

$$\boldsymbol{x}_{n+1} = \arg\max_{x} s_n^2(\boldsymbol{x}) W_n(\boldsymbol{x}) \tag{24}$$

In which case,

$$\mathrm{tMSE}(\boldsymbol{x}_{n+1}) = s_n^2(\boldsymbol{x}_{n+1}) W_n(\boldsymbol{x}_{n+1}) \tag{25}$$

where

$$W_n(\boldsymbol{x}) = \frac{1}{\sqrt{2\pi\left(s_n^2(\boldsymbol{x}) + \varepsilon^2\right)}} \exp\left(-\frac{1}{2}\left(\frac{m_n(\boldsymbol{x}) - T}{\sqrt{s_n^2(\boldsymbol{x}) + \varepsilon^2}}\right)^2\right) \tag{26}$$

The tMSE criterion operates a compromise between regions of high predicted variance (high $s_n^2(\boldsymbol{x})$) and regions located near the predicted frontier controlled by $W_n(\boldsymbol{x})$.

The tuning parameter ε controls the exploration area around the predicted frontier $\tilde{\Gamma} = \{\tilde{y} = T\}$. For instance, $\varepsilon = 0$ forces simulation in a close neighbourhood of the predicted frontier whereas $\varepsilon > 0$ allows a larger exploration. Tuning the value of ε together with smart sampling of candidate points increases the efficiency of the procedure to select new points.

The tMSE criterion can be extended to sample batches of new points based of the constant liar heuristic ([17]) to allow parallel computations.

Once points have been sampled, they are evaluated by the two code levels and added to the database to update the posterior predictive co-kriging distribution $\tilde{y}_2(.)|\boldsymbol{y}$. The probability of conformity, its associated uncertainty and its coefficient of variation are computed according to section 3.6.2 and if the latter is higher than a stopping value, the process of sampling new points is iterated on the updated Gaussian process.

A flowchart of the complete procedure of sequential co-kriging is given at figure 4.

4 Application to the fire engineering case study

In this application, the critical output quantity is the maximum value of the upper layer temperature T_U defined in section 2.4. Non conformity corresponds to $T_U > 200°C$ where the threshold $200°C$ is the tenability threshold defined in section 2.1. The aim of this section is to estimate the probability of non conformity $P(T_U > 200°C)$ and its associated uncertainty with kriging based methods (among them is the sequential co-kriging method), which are respectively denoted $\hat{p}_f$ and $u(\hat{p}_f)$.

4.1 Sensitivity analysis

A sensitivity analysis showed that among the 7 input variables described in table 1, only A_f and $\dot{Q}''$ have an impact on the threshold exceedance.

From now on, the fire engineering case study will thus be treated in a 2D framework in the domain $\mathcal{D} = A_f \times \dot{Q}'' = [1, 20] \times [300, 500]$ with the other variables kept constant.

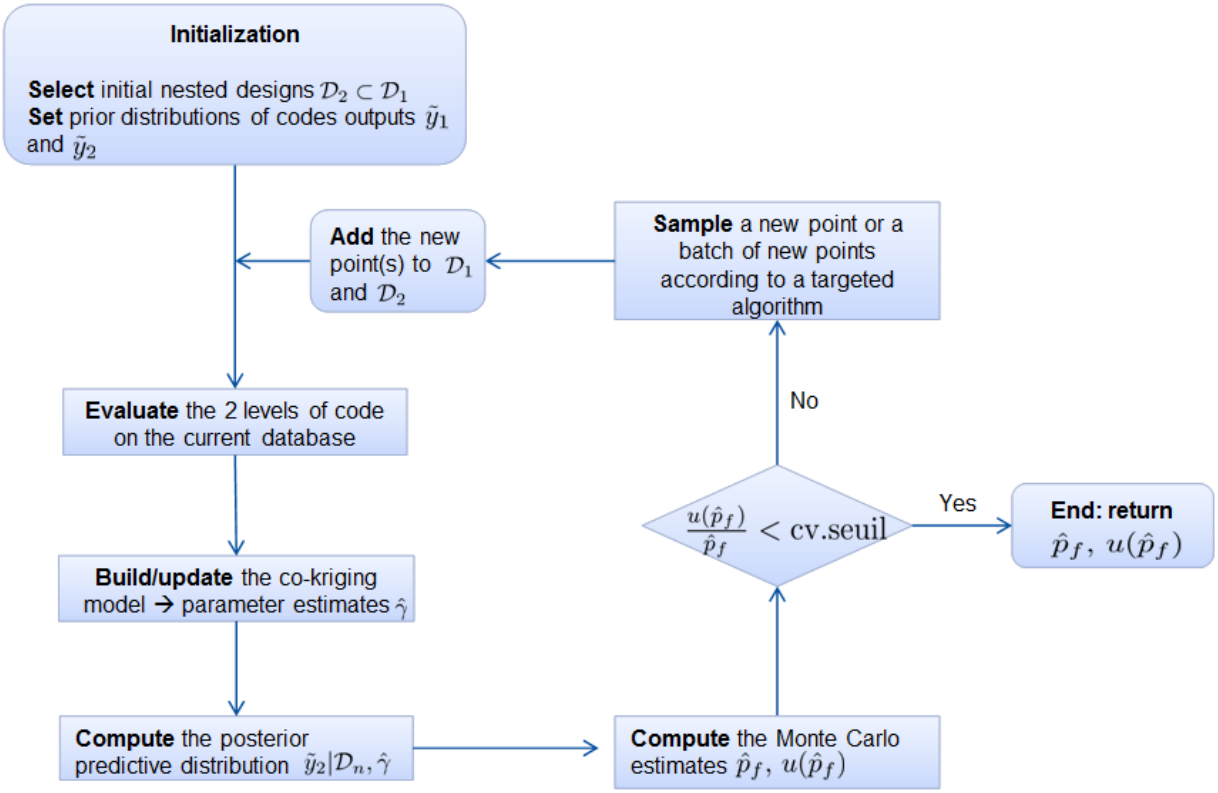

Figure 4: Flowchart of the sequential co-kriging procedure.

4.2 Monte Carlo baseline results

The computation of Monte Carlo estimators of the probability of conformity, its uncertainty and its coefficient of variation is applied to the results of 100 FDS simulations and yields $\hat{p}_f^{MC} = 0.13$, $u(\hat{p}_f^{MC}) = 0.033$ and $cv(\hat{p}_f^{MC}) = \frac{u(\hat{p}_f^{MC})}{\hat{p}_f^{MC}} = 0.25$ respectively.

It follows that nearly $50,000$ runs are required to reach $cv = 1\%$, which is impracticable : if 100 cores/day are available, then the total simulation time amounts to 500 days. Besides, as the sought probability gets smallers, the number of Monte Carlo runs needed increases (for a given cv). For instance, for a probability of 5% reaching $cv = 1\%$ requires more than $200,000$ runs.

In more complex configurations (where 1 run is usually more than 1 week), 100 FDS runs is still too many and only a few simulations can be run.

4.3 Kriging and co-kriging models

Initial database The initial database evaluated by CFAST (F_1)comprises 9 points displayed in figure 5, among them 5 points (in red) are evaluated by FDS (F_2). Voluntarily, no FDS points exceed the threshold.

Parameters of the Gaussian processes Each Gaussian process is modelled with the mean function $h(.) = (1\, A_f)$ to account for the linear effect of A_f on the output, and with the matérn5_2 covariance function to

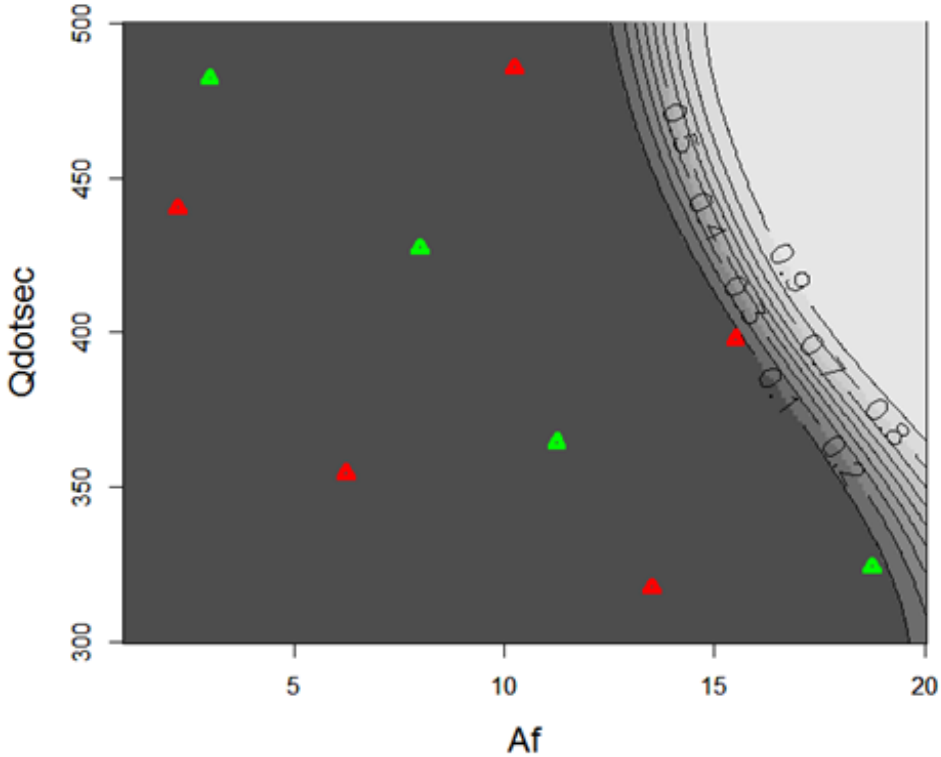

Figure 5: Initial database and initial level plot of the probability of excursion function. In green, the points that are only evaluated by CFAST; in red, the points that are evaluated by CFAST and FDS.

account for smoothness of the output. The matérn5_2 covariance function (see [18]) is defined as a function of $r = |\boldsymbol{x} - \boldsymbol{x'}|$ as

$$k_{\nu=5/2}(r) = \left(1 + \frac{\sqrt{5}r}{\theta} + \frac{5r^2}{3\theta^2}\right) \exp\left(-\frac{\sqrt{3}r}{\theta}\right) \tag{27}$$

where the parameter θ controls the length scale.

The parameters of the co-kriging models have been estimated with the R package MuFiCokriging [19]. The parameters of the kriging models have been estimated with the R package [20].

Number of kriging based Monte Carlo simulations to compute probabilities of non conformity with the notations of section 3.6.2, $K = 1000$ trajectories and $L = 1600$ points on a 40×40 grid.

4.4 Numerical interpretation of the results

Remark In this report, the additional FDS points required to carry out the sequential co-kriging method have been replaced by the predicted mean of the current metamodel of FDS at each iteration. Actual additional FDS points will be displayed in the paper following this deliverable. Thus, the following interpretation of the results should not lead to an overvalued efficiency of the sequential co-kriging method.

A comparison of various kriging based methods has been carried out on the fire engineering case study to show the influence of the number of points in the database and the influence of their location on the estimates of the probability of conformity and its accuracy (relative uncertainty). Results are displayed in table 2.

The point estimate produced by the kriging model ($\hat{p}_f = 0.1349$) built on the 100 points is very close to the point estimate computed with the Monte Carlo method on the same points ($\hat{p}_f = 0.13$). However, the kriging based estimate is much more accurate ($cv(\hat{p}_f) = 0.0416$ versus $cv(\hat{p}_f) = 0.25$). The reason is that kriging based estimates involve a lot of cheap simulations from the metamodel that increase the accuracy of the estimation. It is important to notice that both estimations seem to be biased (much lower values than the sequential co-kriging method) but that the kriging model tends to produce a higher value of the estimate.

For the same number of FDS runs (5 runs) co-kriging reduces the relative uncertainty of the point estimate. A relative uncertainty divided by 3 ($cv(\hat{p}_f) = 0.13$ versus $cv(\hat{p}_f) = 0.3968$) was obtained at the cost of 4 cheap CFAST simulations. This shows the positive impact of combining expensive runs with cheap runs.

Final results of the sequential co-kriging show a dramatic decrease of the relative uncertainty with respect to co-kriging results ($cv(\hat{p}_f) = 0.0078$ versus $cv(\hat{p}_f) = 0.13$) at a cost of only 6 smartly chosen new expensive runs. This relative uncertainty is also much lower than the one obtained with kriging based on 100 expensive runs ($cv(\hat{p}_f) = 0.0078$ versus $cv(\hat{p}_f) = 0.0415$). Besides these results are twice as accurate as the results obtained with 100 expensive FDS simulations ($cv(\hat{p}_f) = 0.13$ versus $cv(\hat{p}_f) = 0.25$).

number of FDS runs	type of analysis	$\hat{p}_f$	$u(\hat{p}_f)$	$cv(\hat{p}_f)$
5	kriging	0.1634	0.0648	0.3968
5	co-kriging	0.172	0.022	0.13
100	kriging	0.1349	0.0056	0.0415
100	Monte Carlo	0.13	0.033	0.25
$5 + 3 \times 2$	sequential co-kriging	0.1710	0.0013	0.0078

Table 2: Summary results of the probability of non conformity $\hat{p}_f$, its associated uncertainty $u(\hat{p}_f)$ and its coefficient of variation (relative uncertainty) $cv(\hat{p}_f)$ obtained with various kriging based methods.

4.5 Graphical interpretation of the sequential co-kriging results

Results obtained at each iteration of the sequential co-kriging procedure (see section 3.7) are displayed in table 3. The first line (iteration 0) gives the co-kriging based Monte Carlo estimates obtained with the initial database (9 points including 5 expensive FDS simulations) displayed at line 2 of table 2.

The contour plot of the posterior probability of excursion function on the full domain provides a graphical tool to assess the efficiency of the iterative algorithm.

The initial contour plot displayed on figure 6a shows a large dispersion of the level lines, representing the uncertainty on the predicted frontier between non conformity (white area) and conformity (black area). For instance the predicted 0.5 line indicates that there is 50% chance that the non conformity domain lies above this line and the predicted 0.9 line indicates that there is 10% chance that the non conformity domain lies above this line.

As points are sequentially added to the database, the uncertainty is reduced. The first two points added (see figure 6b) (red crosses) have a high predicted variance in the target area, as they are far from FDS points (red triangles). Their predicted mean is close to the threshold so that the level lines interpolate the points. The

iteration	number of added points	$\hat{p}_f$	$u(\hat{p}_f)$	$cv(\hat{p}_f)$
0	-	0.172	0.022	0.13
1	2	0.1707	0.0076	0.0446
2	2	0.1709	0.0023	0.0132
3	2	0.1710	0.0013	0.0078

Table 3: Summary results of the probability of non conformity $\hat{p}_f$, its associated uncertainty $u(\hat{p})$ and its coefficient of variation (relative uncertainty) $cv(\hat{p}_f)$ obtained at each iteration of the sequential procedure. Iteration 0 gives the baseline results obtained with the initial database (9 points).

lines are also narrowed in between, close to an initial FDS point, which shows the effect of this point given the additional knowledge.

The next two points added (see figure 7a) have also a predicted mean close to $200°C$ and yield reduced uncertainties so that 1-probability of non conformity zones appear.

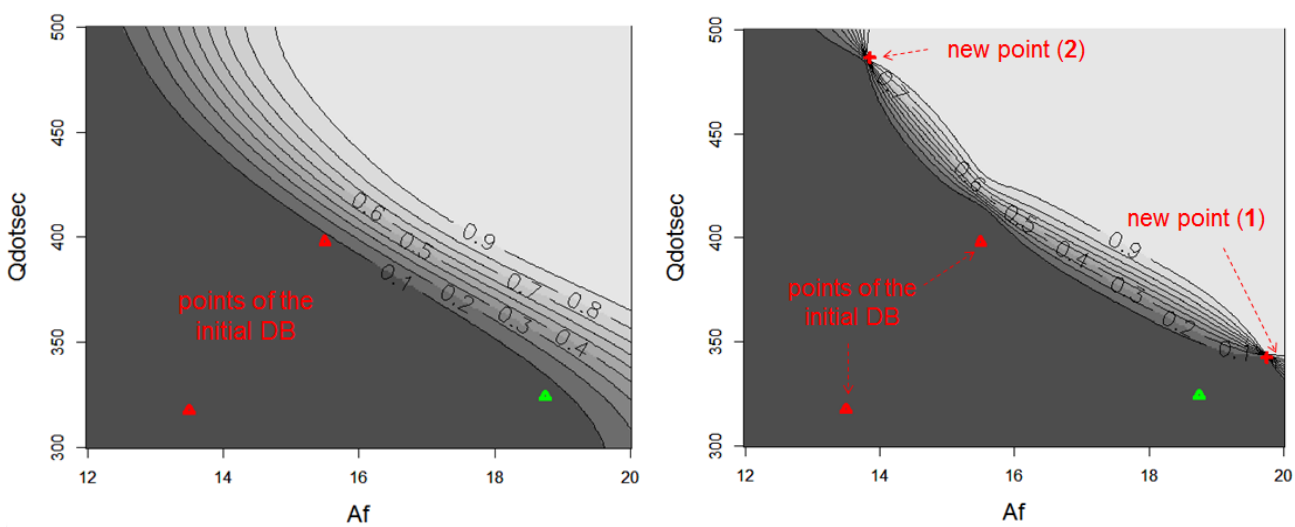

(a) Baseline : points of the initial database

(b) Iteration 1: add 2 points

Figure 6: Contour plot of the initial probability of excursion (a) and the updated probability of excursion after 2 points have been added at the first iteration of the sequential co-kriging procedure (b).

Finally, two more points are needed (see figure 7b) to reach $cv \leq 1\%$, with the effect of creating a 1-probability of non conformity zone, which means that fires starting with coordinates lying in this zone will lead to non conformity ($UL > 200°C$).

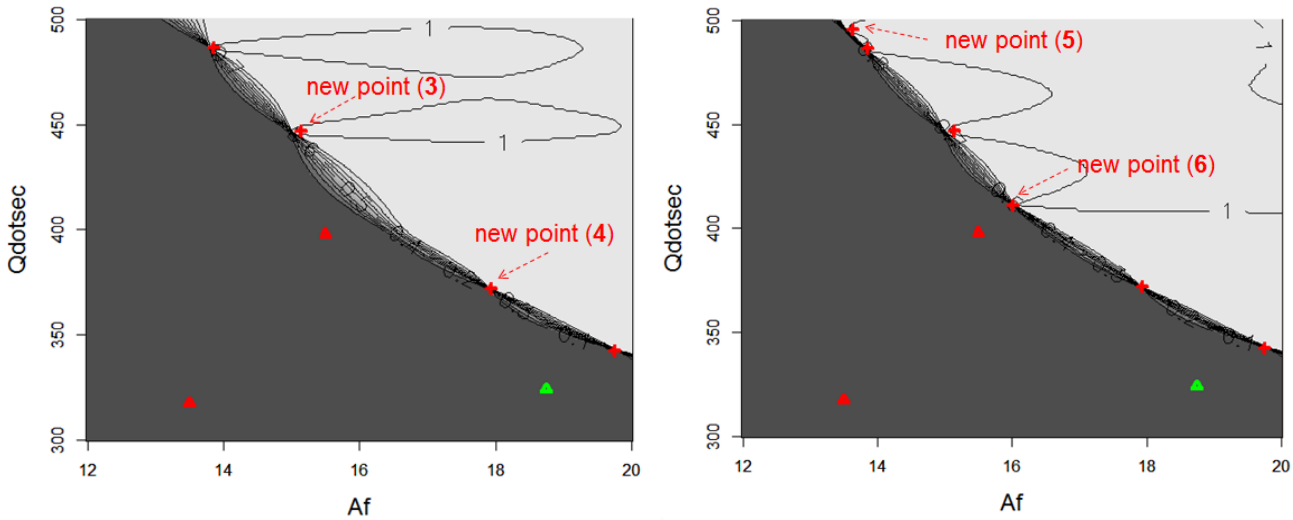

(a) Iteration 2 : add 2 points

(b) Iteration 3 : add 2 points

Figure 7: Contour plot of the updated probability of excursion at the second iteration of the sequential co-kriging procedure (a) and at the third iteration (b).

5 Conclusion

The methodology presented in this document to assess the conformity of an expensive computational code has proved efficient to overcome too parcimonious evaluations from an expensive code when fast approximations are available. This method builds on the kriging models usually used to model code outputs, to improve the predictions of the kriging model of the expensive code. Another desirable feature is that the method allows smart sampling of new points targeting the non conformity domain in order to further reduce the uncertainty of the probability of non conformity. Although demonstrated in a simple but realistic case study, the method is flexible to take into account more complex relationships between the two codes in higher dimensional problems.

Acknowledgements

The EMRP is jointly funded by the EMRP participating countries within EURAMET and the European Union.

References

[1] J. G. M. van der Grinten and A. M. van der Spek. Conformity assessment using monte carlo methods. 16th International Flow Measurement Conference, FLOMEKO 2013, Aug 2013.

[2] P. Carlotti and D. Lamalle. Sensitivity to boundary conditions for simulation of fire plume in enclosure. Proceedings of the 21e congres francais de mecanique, Aug 2013.

[3] D. A. Purser. Assessment of hazard to occupants from smoke, toxic gases and heat. In *SFPE handbook of fire protection engineering*, pages 2.96–2.193. 4th edition.

[4] NF EN ISO 13571 - Guidelines for the estimation of time to compromised tenability in fires. volume ICS: 13.220.01. 2012.

[5] W.W Jones, R.D Peacock, G.P Forney, and P.A Reneke. Cfast - consolidated model of fire growth and smoke transport (version 6), technical reference guide. *NIST SP - 1026*, page 125 pp, 2009.

[6] K. McGrattan, R. McDermott, C. Weinschenk, and K. Overholt. Fire dynamics simulator - technical reference guide, volume 1 mathematical model. *NIST SP - 1018*, page 175 pp, 2014.

[7] Instruction technique, n°246 relative au désenfumage dans les établissements recevant du public, annexe pour le calcul du taux alpha. In *Arrêté du 22 mars 2004*. Documentation BATISS, 2004.

[8] R. L. Alpert. Ceiling jet flows. In *SFPE handbook of fire protection engineering*, pages 2.21–2.36. 4th edition.

[9] D. Drysdale. *An introduction to fire dynamics*. John Wiley, 3nd edition, 2011.

[10] NF EN ISO 7730 - Analytical determination and interpretation of thermal confort using calculation of the pmv and ppd indices and local thermal comfort criteria. volume ICS: 13.18024. 2006.

[11] M.L. Janssens and H.C. Tran. Data reduction of room tests for zone model validation. *Journal of Fire Science*, 201:528–555, 1992.

[12] Y.P. He, A. Fernando, and M.C. Luo. Determination of interface height from measured parameter profile in enclosure fire experiment. *Fire Safety Journal*, 31:19–38, 1998.

[13] M. C. Kennedy and A. O'Hagan. Predicting the output from a complex computer code when fast approximations are available. *Biometrika*, 87:1–13, 1998.

[14] J. Bect, D. Ginsbourger, L. L, V. Picheny, and E. Vazquez. Sequential design of computer experiments for the estimation of a probability of failure. *Statistics and Computing*, 22:773–793, 2012.

[15] J. Oakley and A.O'Hagan. Bayesian inference for the uncertainty distribution of computer model outputs. *Biometrika*, 89:769–784, 2002.

[16] S. Xiong, P.Z.G. Qian, and J. Wu. Sequential design and analysis of high-accuracy and low-accuracy computer codes. *Technometrics*, 55:37–46, 2013.

[17] C. Chevalier, V. Picheny, and D. Ginsbourger. The kriginv package : An efficient and user-friendly r imlementation of kriging-based inversion algorithms. *Computational Statistics and Data Analysis*, 71:1021–1034, 2014.

[18] C. E Rasmussen and C. K. I. Williams. *Gaussian Processes for Machine Learning*. MIT Press, 2006.

[19] Loic Le Gratiet. *MuFiCokriging: Multi-Fidelity Cokriging models*, 2012. R package version 1.2.

[20] Olivier Roustant, David Ginsbourger, and Yves Deville. DiceKriging, DiceOptim: Two R packages for the analysis of computer experiments by kriging-based metamodeling and optimization. *Journal of Statistical Software*, 51(1):1–55, 2012.